



The synthesis, electrochemical and theoretical nonlinear optical properties of push–pull chromophores for photorefractive composites

In Kyu Moon ^{a,*}, Nakjoong Kim ^{b,**}

^a Information and Electronic Materials Lab, Environment and Energy Division, Korea Institute of Industrial Technology, Chungnam 330-825, South Korea

^b Department of Chemistry, Hanyang University, Seoul 133-791, South Korea

ARTICLE INFO

Article history:

Received 2 December 2008

Received in revised form

30 January 2009

Accepted 5 February 2009

Available online 15 February 2009

Keywords:

Chromophores

Dipole moment

Polarizability

Hyperpolarizability

Computation

Photorefractive effect

ABSTRACT

Four chromophores, of different dipole moment and polarizable anisotropy and which comprised conjugation bridges of both benzene and polyene with strong electron-donor and electron-acceptor groups, were characterized using ¹H NMR, FT-IR, UV–vis, and electrochemical analyses. The electric dipole moment (μ), polarizability (α) and the first hyperpolarizability (β) values of the chromophores were examined using computational methods. The contribution of orientational birefringence to total birefringence was estimated from the calculated molecular parameters of the chromophores; these parameters are important factors for predicting photorefractive efficiency.

Published by Elsevier Ltd.

1. Introduction

The nonlinear optical (NLO) character of push–pull type conjugated chromophores has attracted much attention because of their excellent electronic and optical properties. Recently, this class of compounds has also attracted much attention in the field of polymeric PR composites for their large diffraction efficiency and fast response time. The PR effect refers to the spatial modulation of the refractive index of a material due to the light-induced redistribution of the electronic charge. The main characteristics governing the PR are the EO activity and the photoconductivity of a material [1,2]. High performances observed for low- T_g polymers doped with NLO chromophores can be attributed to the efficient orientation of the chromophores in the space-charge field. From this point of view, a good rotational mobility of these molecules is required. The magnitude of the refractive index modulation is determined by the polarizability of the NLO chromophores, their number density in the composite material, and the degree of orientation of these chromophores in the electric field material (external plus space-charge field). The orientational enhancement model proposed by

Moerner and co-workers [3] provided an explanation for the high performance of these materials. The resulting orientational effects observed in low- T_g polymers have led to a new FOM for the optimization of chromophores for photorefractive applications:

$$\text{FOM} = \frac{1}{M} \left[9\mu_0\beta + \frac{2\mu_0^2\Delta\alpha}{k_B T} \right] \quad (1)$$

where kT is the thermal energy, $\Delta\alpha$ the anisotropy of the molecular polarizability, μ_0 the undressed dipole moment of the molecule, and β the first hyperpolarizability. The first term of Eq. (1) is related to the Pockels effect (F_{Pockels} , <25%) while the second term corresponds to the orientational birefringence (F_{BR} , >75%) [1,2,4]. Also, PR chromophores with small molecular and large dipole moment according to the operating wavelengths are crucial to the advancement of PR materials, and have drawn interest in their theory-guided design and state-of-the-art synthesis. Among them, a series of highly polarizable chromophores based on strong-acceptor-substituted aromatic chromophores have demonstrated very large $\Delta\alpha$ values [1]. As a consequence, the design criteria for the favorable chromophore of low- T_g PR polymer system diverge from those for inorganic crystal and high T_g electro-optic polymer [2,5]. In the view of an enhancement of orientational birefringence, the recent research concentrates on the optimization of the dipole moment (μ) and polarizability anisotropy ($\Delta\alpha$) of the chromophore.

* Corresponding author. Tel.: +82 41 5898 522; fax: +82 41 5898 580.

** Corresponding author.

E-mail addresses: inkmoon@naver.com (I.K. Moon), kimnj@hanyang.ac.kr (N. Kim).

However, in addition to the optical nonlinearity related with $\mu^2\Delta\alpha$, a few more things have to be taken into account in chromophore design for a PR material. The first thing is the device stability of a material. Frequently the increase of dipole moment of a chromophore accompanies the reduction of solubility in a nonpolar photoconducting medium, *i.e.* PVK. ATOP [6], this is known as one of the most appropriate chromophores for the area of PR polymers. Another important aspect of chromophore design is that photoconductivity of a PR material is strongly dependent on the chromophore. Many researchers have reported that the charge mobility of PR polymer is greatly suppressed by the addition of chromophore, depending on its concentration, ionization potential, dipole moment and so on [2,7]. Since the process of space-charge field formation is closely related with the photoconductivity, the response time of PR polymers is greatly influenced by the property of the chromophore doped in photoconducting medium.

The present work describes the UV–vis spectra and electrochemistry studies of the newly synthesized NLO chromophores, to understand the relationship between the molecular structural features and NLO properties. Requirements for the large PR effect are a large FOM for the birefringent or electro-optic response. Since the characterization of the molecular conformation and the charge distribution of the chromophores studied are essential to complete understanding of NLO properties, we used PM3 method in order to perform structural analysis and to predict PR performance. Our work deduces also that increasing the strength of conjugation length and acceptor moieties attached to a conjugated linker can result in the enhancement of the first hyperpolarizability.

2. Experimental

2.1. Instrumentation

Proton NMR spectral analyses were performed on a Varian Technology 300/54 System spectrometer. ^1H NMR spectra were obtained in deuterium solutions with tetramethylsilane internal standards unless otherwise noted. Infrared spectra were obtained on a Perkin Elmer spectrometer Paragon 1000 PC and frequencies were given in reciprocal centimeters. An Optizen UV/VIS Spectrometer was used for UV–vis spectral data. The electrochemical experiments were carried out using the 237A EG & G Princeton CV device. The voltammograms were obtained at 25 °C in anhydrous acetonitrile containing 2 mM tetra-*n*-butylammonium tetrafluoroborate acetonitrile ($n\text{-Bu}_4\text{NBF}_4$) at a scan rate of 100 mV s $^{-1}$ under nitrogen atmosphere. The working electrode was platinum (Pt). The potentials were recorded against a Ag/AgCl as reference electrode and each measurement was calibrated with ferrocene/ferrocenium (Fc) redox system as an internal standard.

2.2. Materials

All reagents and solvents were purchased from Aldrich and TCI, and used without further purification unless otherwise noted. DMF and halogen solvents were stored over molecular sieves. THF and toluene were distilled over sodium benzophenone ketyl. All other solvents were distilled from calcium hydride unless otherwise noted. K_2CO_3 was dried under vacuum at 150 °C. All reactions involving organometal reagents were carried out under dry, oxygen-free nitrogen and reagents were transferred with syringes through a rubber septum cap fitted to the reaction flask.

2.2.1. 4-Bis(*n*-butylamino)benzaldehyde (ABA)

A two-necked 100 mL flask, fitted with a condenser, was charged with 3.0 g (24.2 mmol) of 4-fluorobenzaldehyde, 3.75 g (29.0 mmol) of *n*-dibutylamine, 6.68 g (48.3 mmol) of potassium

carbonate, Aliquat $^{\text{®}}$ 336 (1 drop) and 70 mL DMF. The resulting solution was stirred at 80 °C for 3 days. After cooling to room temperature, the mixture was put into 500 mL of distilled water and extracted three times with ethyl acetate (3 \times 50 mL). The combined organic fractions were dried over magnesium sulfate and the solvent was removed under reduced pressure. The crude material was purified by column chromatography (silica gel, hexane–5% ethyl acetate as eluent) to give 73% of the title product. ^1H NMR (CDCl_3 , ppm) δ 0.98 (t, 6H), 1.35 (tq, 4H), 1.59 (tt, 4H), 3.34 (t, 4H), 6.63 (d, 2H), 7.69 (d, 2H), 9.69 (s, 1H). FT-IR (KBr pellet, cm^{-1}) 1750 (C=O), 2754 (C–H $_{\text{ald}}$). Anal. Calcd for $\text{C}_{15}\text{H}_{23}\text{NO}$: C, 77.21; H, 9.93; N, 6.00. Found: C, 77.43; H, 10.13; N, 6.17.

2.2.2. 2-(3,5,5-Trimethyl-2-cyclohexenyliden)malononitrile (DCI)

Into a three-necked flask equipped with a nitrogen inlet, a Dean–Stark trap, and a condenser, were placed 3 g (21.7 mmol) of isophorenone, 1.58 g (23.9 mmol) of malononitrile, 0.56 g (7.3 mmol) of ammonium acetate and acetic acid (2 mL) with 60 mL of benzene. The mixture was heated while stirring at 100 °C under a thin stream of nitrogen to remove the by-product of water by azeotropic distillation with benzene for 12 h. After the benzene had been removed, the mixture was poured into water, 1 M aqueous of sodium bicarbonate and extracted three times with ethyl acetate (50 mL \times 3). The combined organic fractions were dried over magnesium sulfate and the solvent was removed under reduced pressure. The crude material was purified by column chromatography (silica gel, hexane–10% ethyl acetate as eluent) to give 94% of the title product. ^1H NMR (CDCl_3 , ppm) δ 1.00 (s, 6H), 2.02 (s, 3H), 2.08 (s, 2H), 2.52 (s, 2H), 6.61 (s, 1H). FT-IR (KBr pellet, cm^{-1}) 1750 (C=O), 2754 (C–H $_{\text{ald}}$). Anal. Calcd for $\text{C}_{12}\text{H}_{14}\text{N}_2$: C, 77.58; H, 7.58; N, 15.04. Found: C, 77.87; H, 15.19; N, 15.21.

2.2.3. 2-Dicyanomethylene-3-cyano-4,5,5-trimethyl-2,5-dihydrofuran (TCF)

This was synthesized as previously described [8,9]. ^1H NMR (CDCl_3 , ppm) δ 1.60 (s, 6H), 2.36 (s, 3H). Anal. Calcd for $\text{C}_{11}\text{H}_9\text{N}_3$: C, 66.32; H, 4.55; N, 21.09. Found: C, 66.0; H, 4.67; N, 21.29.

2.2.4. 5-[[4-(Dibutylamino)phenyl]methylene]-1-ethyl-4-methyl-2,6-dioxo-1,2,5,6-tetrahydro-3-pyridinecarbonitrile (A)

A 50 mL flask was charged with 0.77 g (4.3 mmol) of 1-ethyl-1,2-dihydro-6-hydroxy-4-methyl-2-oxo-3-pyridinecarbonitrile (1.0 equiv), 1.0 g (4.3 mmol) of ABA, and 20 mL of acetic anhydride. The mixture was stirred under nitrogen atmosphere at 110 °C for 3 h. After cooling to room temperature, the solvent was removed under reduced pressure. The crude material was passed through a short column of silica gel using chloroform as eluent. The compound was dissolved in a hot ethanol. After cooling to 0 °C, the solid was recovered by filtration to provide 71% of the title product. ^1H NMR ($\text{DMSO}-d_6$, ppm) δ 0.93 (t, 6H), 1.09 (m, 6H), 1.37 (m, 4H), 1.57 (m, 4H), 2.16 (s, 2H), 6.83 (d, 2H), 7.82 (s, 1H), 8.29 (d, 2H). Anal. Calcd for $\text{C}_{24}\text{H}_{31}\text{N}_3$: C, 73.25; H, 7.94; N, 10.68. Found: C, 73.43; H, 7.79; N, 10.87.

2.2.5. 2-{3-Cyano-4-[2-(4-dibutylamino-phenyl)-vinyl]-5,5-dimethyl-5H-furan-2-ylidene}-malononitrile (B)

A 50 mL flask was charged with 0.85 g (4.3 mmol) of TCF (1 equiv), 1.0 g (4.3 mmol) of ABA, and 30 mL of ethanol. Then, 2 drops of piperidine was added, and the mixture was stirred overnight at 80 °C. After cooling to room temperature, the solvent was removed under reduced pressure. The crude material was passed through a short column of silica gel using hexane–95% chloroform as eluent. The compound was dissolved in hot ethanol. After cooling to 0 °C, the solid was recovered by filtration to provide 41% of the title product. ^1H NMR (CDCl_3 , ppm) δ 0.98 (t, 6H), 1.38 (m, 4H), 1.63 (m, 4H), 1.73 (s, 6H), 3.39 (t, 4H), 6.67 (d, 2H), 6.74 (d, 1H), 7.53

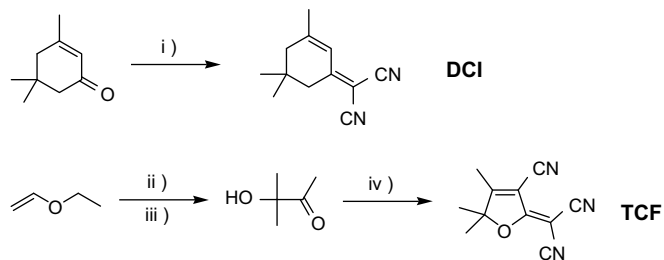


Fig. 1. Synthetic route of different withdrawing groups. Reaction conditions: (i) malonitrile/ $\text{CH}_3\text{CO}_2\text{NH}_4/\text{CH}_3\text{CO}_2\text{H}/\text{benzene}$; (ii) $t\text{-BuLi}/\text{THF}$; (iii) acetone; (iv) malonitrile/sodium ethoxide/abs. ethanol.

(d, 2H), 7.61 (d, 1H). Anal. Calcd for $\text{C}_{26}\text{H}_{30}\text{N}_4$: C, 75.33; H, 7.29; N, 13.52. Found: C, 75.31; H, 7.19; N, 13.78.

2.2.6. 2-[3-[(E)-2-(Piperidino)-1-ethenyl]-5,5-dimethyl-2-cyclohexenylidene]malononitrile (C)

A two-necked 25 mL flask, fitted with a condenser, was charged with 1 g (5.4 mmol) of **DCI** and 5 mL of 4-piperidinoformamide dimethyl acetal (20 mL) [10]. The resulting solution was degassed with a vigorous flow of nitrogen for 30 min, and then the mixture was heated at 90°C for 3 h under nitrogen atmosphere. The mixture was allowed to cool to room temperature and the volatile components were removed using a rotary evaporator. The crude material was passed through a short column of silica gel using chloroform as eluent. Recrystallization from ethanol afforded 87% of the title product. ^1H NMR (CDCl_3 , ppm) δ 1.01 (s, 6H), 1.68 (br s, 6H), 2.26 (s, 2H), 2.47 (s, 2H), 3.33 (br s, 4H), 5.40 (d, 1H), 6.36 (s, 1H), 7.02 (d, 1H). FT-IR (KBr pellet, cm^{-1}) 2202 ($\text{C}\equiv\text{N}$). Anal. Calcd for $\text{C}_{18}\text{H}_{23}\text{N}_3$: C, 76.83; H, 8.24; N, 14.93. Found: C, 77.11; H, 8.36; N, 14.71.

2.2.7. Dicyanomethylene-3-cyano-5,5-trimethyl-(dimethylamino)vinyl-2,5-dihydrofuran (D)

This compound was synthesized according to a similar procedure described previously for the synthesis of compound **C** using

TCF with N,N -dimethylformamide dimethyl acetal. The crude material was purified by crystallization in THF–hexane to give 92% of the title product. ^1H NMR (CDCl_3 , ppm) δ 1.62 (s, 6H), 2.87 (s, 6H), 4.95 (d, 1H), 6.80 (d, 1H). Anal. Calcd for $\text{C}_{14}\text{H}_{14}\text{N}_4$: C, 66.13; H, 5.55; N, 22.03. Found: C, 66.29; H, 5.44; N, 22.20.

3. Results and discussion

3.1. Synthesis and characterization

It has been reported that for the NLO chromophore, the extension of the conjugation length and introduction of electron-withdrawing groups at the terminal positions(s) result in an improvement of the NLO properties. Figs. 1 and 2 show the chemical structures of chromophores synthesized in this work. The chromophores' structures were varied by using different types of π -conjugation bridges such as polyene and benzene combined with electron acceptors. The most convenient method to introduce withdrawing groups at the terminal positions of chromophore synthesis is the Knoevenagel type condensation of the aldehyde (ketones) with malononitrile. The chromophores were synthesized using two different donor bridge systems which consist of a dialkylaminobenzene and a dialkylaminopolyene donor. Synthesis of the electron acceptors was accomplished following the general procedures outlined below. **DCI** and **TCF** were synthesized according to a well-known method. These products then reacted with the electron donors (**ABA** and aminodiacetal). Their chemical structures were identified by FT-IR and ^1H NMR spectroscopy. The aldehyde group in **ABA** was also identified by the peak at 9.69 ppm in the ^1H NMR spectrum. In all the electron-acceptor groups (**DCI**, **TCF**), the stretching band of the cyano group was identified at $\sim 2205\text{ cm}^{-1}$ in FT-IR spectra. The starting $-\text{CHO}$ peak of **ABA** at 1745 cm^{-1} completely disappeared with the electron-accepting groups by Knoevenagel reaction. Final products of chromophores were easily prepared by the reactions of the electron parts and the electron-acceptor parts, which were confirmed by aromatic and

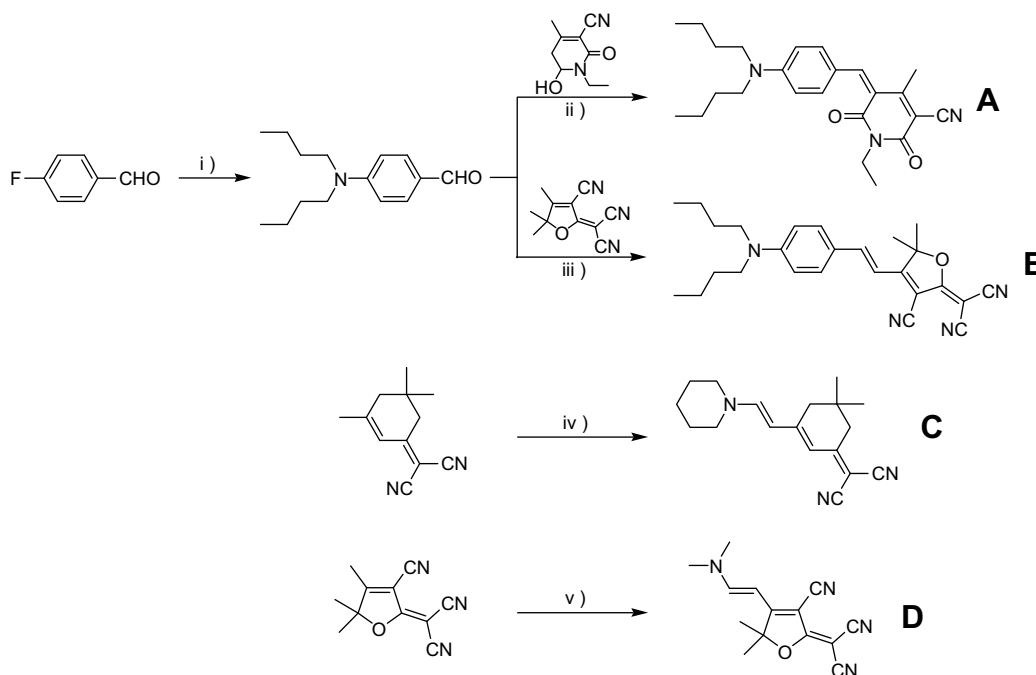


Fig. 2. Synthesis of NLO chromophores. Reaction conditions: (i) n -dibutylamine/ $\text{K}_2\text{CO}_3/\text{DMF}$; (ii) acetic anhydride; (iii) cat. piperidine/ethanol; (iv) 4-piperidinoformamide dimethyl acetal (v) N,N -dimethylformamide dimethyl acetal.

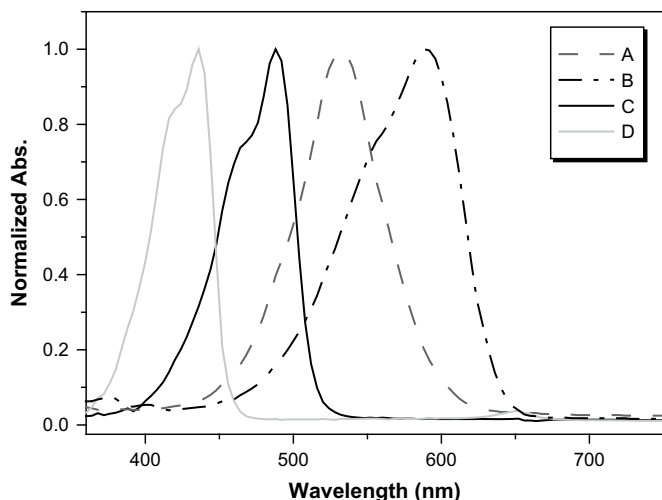


Fig. 3. UV-vis spectra of NLO chromophores in methylene chloride.

vinyl (polyene) protons at ~ 5.37 to ~ 8.35 ppm in ^1H NMR spectra and the absorption peaks of cyano group at $\sim 2197\text{ cm}^{-1}$ in FT-IR spectra.

The UV-vis absorption of chromophores **A**, **B**, and **D** in methylene chloride is shown in Fig. 3 and Table 1, together with that of **C** [11] for comparison. An increase in acceptor strength induces a bathochromic shift of the λ_{max} as expected. In general, the maximum absorption wavelength depends on the strength of the donor/acceptor pair. As expected the bathochromic shift is largest for chromophores containing **TCF**, compared to 1-ethyl-4-methyl-2,6-dioxo-1,2,5,6-tetrahydropyridine-3-carbonitrile, and **DCI** acceptors. The series of chromophores exhibits intense π - π^* transitions with charge-transfer character in the visible region between 436 and 588 nm. The position of this band is strongly influenced by the structure of the compounds, for example by the type of substitution pattern in the donor and the acceptor moieties. We found that increasing either the acceptor strength or the length of the π -conjugation bridge caused a red-shift. The maximum absorption wavelength depends on the strength of the donor/acceptor pair. Chromophore **B** (588 nm) showed a nearly 56 nm red-shift in λ_{max} compared with chromophore **B** (532 nm) due to a stronger acceptor group, **TCF** [12–14]. This effect has been attributed to the stabilization of LUMO by the electron-withdrawing groups [15]. However, chromophore **D** (436 nm) was 52 nm shorter than that of chromophore **C** (488 nm). When the π -conjugation bridge of **D** becomes much shorter, the acceptor does not preferentially shift. This observation is apparently due to a shorter π -conjugation bridge of **D** and less efficient electron acceptance of **TCF** in our case. That is, it is found that chromophore **C** shows more red-shifted than that of **D**, which is attributed to the

positive contribution of their elongated conjugation length. In general, the stronger the donor and/or acceptor group, the smaller the energy difference between ground and excited states, and the longer the wavelength of absorption [16]. The energy levels of the NLO chromophore are the driving force of the charge mobility in polymeric PR composite due to acting as a trap for photoconductive medium, e.g., PVK. If the HOMO of the NLO chromophore is higher in energy than that for the charge-transport molecule, the chromophore can donate an electron from its HOMO to a nearby charge-transport molecule HOMO. Thus, the chromophore HOMO as a hole trap can affect the charge mobility, which in turn affects the photoconductivity, with lower photoconductivity for deeper hole traps [7]. We performed electrochemical analysis to determine the ionization potentials of the chromophores (Fig. 4).

Voltammograms of $\sim 10^{-3}\text{ M}$ CH_3CN solutions of chromophores are shown in Fig. 4, and the data are listed in Table 1. CV at a scan rate of 100 mV s^{-1} was the electrochemical technique applied to study the oxidation behavior of chromophores. The one-electron oxidation reaction was found to be typically Nernstian for chromophore **B**, whereas that for chromophores **A**, **C**, and **D** was irreversible oxidation. Chromophores **A**, **C**, and **D** show a single irreversible peak on the first positive scan to give the resonance-stabilized amino radical cation. In an oxidative potential region, a p-doping peak gives a reversible one-electron oxidation at $+965.15\text{ mV}$ (irreversible $E_p = +1056\text{ mV}$) vs. Ag^+/Ag for chromophore **B**. The p-doping is considered to occur mainly at the donor unit, and the order of the p-doping potential is considered to reflect electron-donating ability (or ionization potential) of the amine unit. On the other hand, chromophores **A**, **C**, and **D** exhibit only an irreversible oxidation potential ($E_p = +650, +1057$, and $+1413\text{ mV}$), which is considered to be due to the electron-donating effects of the amino group and a strong interaction of the anion dopant (BF_4^-) with the amine group. An irreversible oxidation peak of chromophore **A** lies energetically higher than the other chromophores. The most remarkable result of this study is the high oxidation potential ($+1413\text{ mV}$) due to the very short chain lengthening. This effect is clearly observed in chromophores, which incorporate acceptors of different strength via conjugation length, and agrees with the general trend observed for other related structures [17,18]. The energy levels of the HOMO and the LUMO were thus estimated from the cyclic voltammograms and the onset of the absorption spectra. The results are summarized in Table 1. The oxidation process corresponds to the removal of electrons from the HOMO, whereas the LUMO is calculated with optical energy gap from the absorption edge of the electronic spectrum. Therefore, this can provide important information regarding the magnitude of the energy gap. Chromophore **D** had the lowest HOMO level (-6.06 eV). Chromophore **C**, which has an electron-donating amine group on the polyene unit, had a higher HOMO level (-5.35 eV) than that of **B** and **A**. The LUMO of chromophore **C** was higher in energy than that of other chromophores. This can be explained on

Table 1
Optical and electrochemical properties of NLO chromophores.

Phore	λ_a^a nm (ϵ , $\text{M}^{-1}\text{ cm}^{-1}$)	Cyclic voltammetry		Absorption spectroscopic data	
		Oxidation potential ^b (V)	HOMO ^c (eV)	LUMO ^d (eV)	Optical energy gap ^e (eV)
A	532 (16,670)	1.057	-5.57	-3.52	2.05
B	588 (32,160)	1.056	-5.73	-3.80	1.93
C	488 (24,407)	0.650	-5.35	-2.94	2.41
D	436 (21,532)	1.413	-6.06	-3.34	2.72

^a Maximum wavelength of λ_{abs} in methylene chloride.

^b Irreversible oxidation potential values were measured by cyclic voltammetry in an acetonitrile solution of $[(\text{C}_2\text{H}_5)_4\text{N}]\text{BF}_4$ (0.10 M).

^c HOMO energy values were calculated using ferrocene value of 4.8 eV below the vacuum level.

^d LUMO energy values were calculated from the HOMO level and optical band gap.

^e Optical band gaps taken as the absorption edges of the UV-vis spectra of the chromophore solutions.

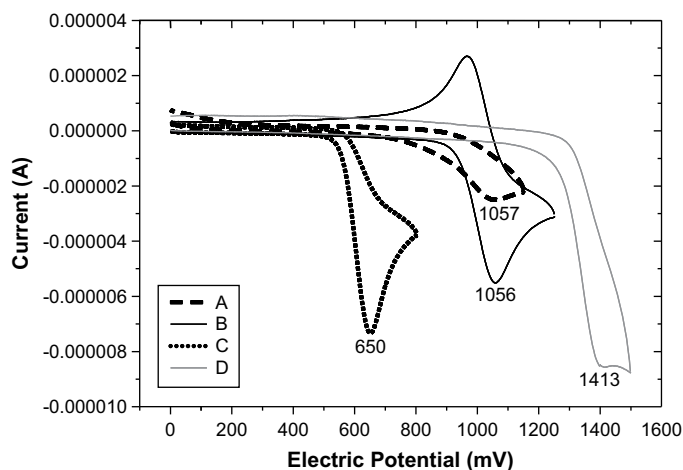


Fig. 4. Cyclic voltammograms of the anodic oxidation of A, B, C, and D chromophores.

the basis that the polyene structure decreases the π -density, coupled with the strong electron-accepting ability of dicyano-group via the strong electron-donating ability of the amino group. This observation has predicted that the former can act as a more

effective hole trap, *i.e.* carbazole radical cation, which reduces the photoconductivity with increased trapping in the polymeric PR composite [11,19]. Thus, at the PVK doped with chromophore D, photoconductivity is expected to increase due to the higher ionization potential energy of chromophore D (HOMO = -6.06 eV, LUMO = -3.34 eV) compared to PVK (HOMO = -5.7 eV, LUMO = -2.2 eV) [20]. In comparison of the energy band gap, the chromophore containing the TCF unit showed lower value than that of the chromophore. Increasing the length of conjugation and the introduction of additional accepting ability of the TCF of the HOMO–LUMO gap are shown in Table 1.

3.2. Molecular studies

The optimized three-dimensional structures from the edge view of π -plane of chromophores are obtained by the Hartree–Fock calculation with the Slater Type Orbital-3 Gaussian basis set in Gaussian 98 software as shown in Table 2 [21]. The three-dimensional structure may help to prevent intermolecular electrostatic interactions among the chromophores, which in turn may enhance the poling efficiency and decrease the scattering-induced optical loss [22,23]. Most significantly, the whole of molecular is close to planar. The dihedral angle between the phenyl-methylene plane (C3 and C4)

Table 2
Optimized structures from the space-filling view of π -plane and HOMO–LUMO surfaces of chromophores were calculated at the theory level HF using the STO-3G basis set using the Gaussian 98 program package (Gaussian Inc.).

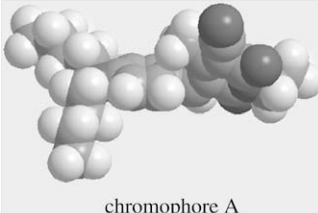
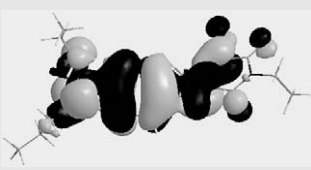
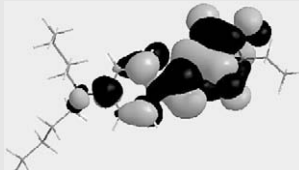
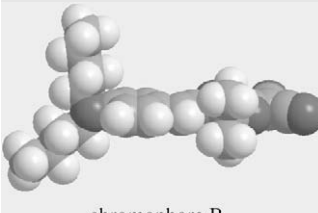
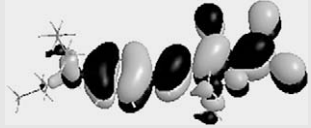

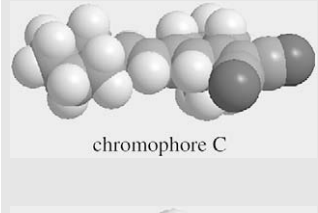

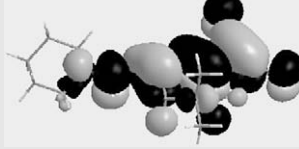



Space-filling view	HOMO	LUMO
 chromophore A		
 chromophore B		
 chromophore C		
 chromophore D		

Table 3

Dipole moment (μ), polarizability anisotropy ($\Delta\alpha$) and hyperpolarizability (β) calculated from MOPAC 6 in CAChe program and estimated FOM of chromophores.

Chromophore	A	B	C	D
M (kg mol ⁻¹)	0.393	0.414	0.281	0.254
$ \mu $ (10 ⁻³⁰ C m)	24.00	37.87	24.30	36.65
$ \Delta\alpha $ (10 ⁻⁴⁰ C m ² V ⁻¹)	43.18	51.28	31.95	30.61
$ \beta $ (10 ⁻⁵⁰ C m ³ V ⁻²)	20.19	37.37	14.37	10.99
F_{BR} (10 ⁻⁷⁷ C ² m ⁴ mol V ⁻² kg)	35.20	98.6	37.3	89.8
$F_{Pockels}$ (10 ⁻⁷⁷ C ² m ⁴ mol V ⁻² kg)	11.1	30.8	11.2	14.3

and the electron-acceptor plane (C17) is 130.98° for chromophore **A** and the dihedral plane is twisted the plane as dogleg-type geometry. The molecular twist can be attributed to the repulsion between the groups attached to the 4-methyl group on 1-ethyl-4-methyl-2,6-dioxo-1,2,5,6-tetrahydropyridine-3-carbonitrile system and the *meta*-hydrogen atoms on the aminobenzene system. In Table 2, the chromophores B–D show an almost perfect coplanar arrangement between the donor group and the acceptor group.

The push–pull chromophores have been a special interest to many investigators because of their relatively large molecular hyperpolarizability β due to delocalization of the π -electronic clouds. The calculated HOMO and LUMO surfaces of the chromophores **A**, **B**, **C**, and **D** have structures in the energy-minimized gas-phase geometry. Table 2 shows HOMO–LUMO of chromophores accompanying electronic excitation to the first excited state. We can see a strong delocalization of both HOMO and LUMO on the π -conjugation bridge. The qualitative pictures clearly prove a net flow of electron density (intramolecular charge transfer) from the electron-donor group by way of the π -electron bridge to the electron-acceptor group. The electron-acceptor groups display positive charges, while the electron-donor groups display negative ones. The HOMO is delocalized on the chromophore's overall framework; the LUMO is highly localized on the electron-acceptor groups. Since large π -electron deficiency arises at the *p*-position, attaching an electron donor group here stabilizes the excited state and lowers its energy relative to the ground state, resulting in the bathochromic shift of the corresponding absorption band (Fig. 1).

The PR quality of some NLO chromophores to be used in high performance PR polymer composite has large dipole moments and large anisotropy of the linear polarizability. It was well known that the higher values of dipole moment, molecular polarizability, and

hyperpolarizability are important for more active NLO properties. Key parameters of these chromophores can be estimated based on the PR FOM according to Eq. (1). FOM parameter is an important factor for predicting PR efficiency. Dipole moment (μ), molecular polarizability anisotropy ($\Delta\alpha$), and hyperpolarizability (β) of chromophore were calculated using the semi-empirical method, MOPAC 2005 by PM3 approximation method for geometry optimization [24]. The calculated molecular electronic parameters (μ , $\Delta\alpha$, and β), and F_{BR} and $F_{Pockels}$ are summarized in Table 3. The dipole moments of the chromophores are large and lie in the range 24–36.65 $\times 10^{-30}$ C m. A comparison of the NLO chromophores of FOM with the theoretically calculated μ values shows that the chromophores **B** and **D** performed better than the chromophores **A** and **C**. In our calculations, it is found that the μ of the four types of chromophores was in the order $\mu(\mathbf{B}) > \mu(\mathbf{D}) > \mu(\mathbf{C}) > \mu(\mathbf{A})$. In the case of chromophore **A**, the lowest dipole moment may be due to the steric repulsion, and this distortion from planarity along the π -conjugation bridge causes to reduce the extent of π -orbital conjugation and thus decreased μ value compared to chromophore **B**. In contrast, chromophore **D** possessed higher dipole moment than chromophore **C** due to a short distance between the donor and acceptor. The polarizability (α) of four chromophores was about 30.61–51.28 $\times 10^{-40}$ C m² V⁻¹, which was a little higher value than that 22 $\times 10^{-40}$ C m² V⁻¹ of DMNPAA [25], leading to a larger linear polarizability anisotropy (larger birefringence). Many π -conjugated systems with a single donor–acceptor substitution exhibit intense low-lying charge-transfer transitions. The polarizability increased with the bond-length alternation reduction, indicating that strong donors and acceptors lead to large linear polarizability for push–pull chromophores [26,27]. In order to investigate NLO potentials of these chromophores, we calculated their hyperpolarizability. It is well known that the higher values of $\mu\beta$ are important for more active NLO properties. In general, the increase of the β values characteristic of the nonlinear optical effect is accompanied by an increase of the λ_{max} in the UV–vis spectra, *i.e.* a decrease in the intramolecular charge-transfer values [28]. The β of four chromophores was about 10.99–37.37 $\times 10^{-50}$ C m³ V⁻², which was a lower value than that 56 $\times 10^{-50}$ C m³ V⁻² of DMNPAA. This is attributed to more stable chemical structure of our chromophore itself with higher conjugation energy [29]. However, chromophore **B** has the value of β : 37.37 $\times 10^{-50}$ C m³ V⁻², which is larger than that of chromophores **A**, **C**, and **D**. Therefore, a relationship between λ_{max} and β has been considered as a fundamental property of π -conjugated system donor–acceptor interactions. Large β values can be obtained by increasing the conjugation length and strength of the donor and acceptor groups (Fig. 5). For one-dimensional push–pull chromophores, either increasing the conjugation length or changing the π -conjugation system inevitably results in enhancement of their charge-transfer properties.

The calculated results show that F_{BR} was an order of magnitude larger than $F_{Pockels}$, which means that the contribution of birefringence presumably play the major role in the refractive index modulation via orientation enhancement effect in low- T_g materials, as found in the literature [1,5,11]. In our calculations, it is found that the F_{BR} of the four types of chromophores was in the order **B** > **D** > **C** ~ **A**. These chromophores had the sufficient NLO properties compared to the reported NLO chromophores and thus can be good candidates for the PR chromophores.

4. Conclusion

Various push–pull NLO chromophores have been synthesized for the development of PR composites. In these chromophores, the donor group is an electron-rich amine while the acceptor group is the electron-poor heterocycle and cyano groups. Chromophore

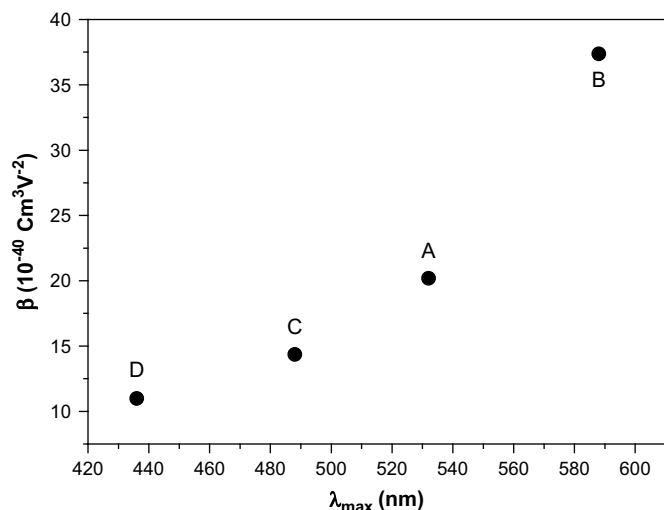


Fig. 5. β vs. λ_{max} of chromophores **A**, **B**, **C**, and **D**.

properties in solution were investigated by combining UV–vis and electrochemical (CV) measurements. Chromophore **D** had the lowest HOMO level. The μ , α , and F_{BR} of four chromophores were calculated using the PM3 method. Results of our calculations show that all these chromophores possessed a PR FOM. The best birefringence should be chromophores **B** and **D** ($F_{BR} = 98.6 \times 10^{-77}$ and $89.8 \times 10^{-77} \text{ C}^2 \text{ m}^4 \text{ mol V}^{-2} \text{ kg}$ respectively). We expect further improvement on the performance and stability of PR composite devices in the near future via optimizing the chromophore properties.

Acknowledgements

This work was supported by the Korea Science and Engineering Foundation (KOSEF) grant funded by the Korea government (MEST) (No. R11-2007-050-01003-0). In addition, this work was supported by the Research fund of HYU (HYU-2008-T).

References

- [1] Würthner F, Wortmann R, Meerholz K. Chromophore design for photorefractive organic materials. *Chemphyschem* 2002;3:17–31.
- [2] Ostroverkhova O, Moerner WE. Organic photorefractives: mechanisms, materials, and applications. *Chemical Reviews* 2004;104:3267–314.
- [3] Moerner WE, Silence SM, Hache F, Bjorklund GC. Orientationally enhanced photorefractive effect in polymers. *Journal of the Optical Society of America B* 1994;11:320–30.
- [4] Wortmann R, Poga C, Twieg RJ, Geletneký C, Moylan CR, Lundquist PM, et al. Design of optimized photorefractive polymers: a novel class of chromophores. *The Journal of Chemical Physics* 1996;105:10637–47.
- [5] Chun H, Moon IK, Shin D-H, Song S, Kim N. The effect of the molecular structure of the chromophore on the photorefractive properties of the polymer system with low glass transition temperatures. *Journal of Materials Chemistry* 2002;12:858–62.
- [6] Würthner F, Yao S, Schilling J, Wortmann R, Redi-Abshiro M, Mecher E, et al. ATOP dyes. Optimization of a multifunctional merocyanine chromophore for high refractive index modulation in photorefractive materials. *Journal of American Chemical Society* 2001;123:2810–4.
- [7] Hendrickz E, Zhang Y, Ferrio KB, Herlocker JA, Anderson J, Armstrong NR, et al. Photoconductive properties of PVK-based photorefractive polymer composites doped with fluorinated styrene chromophores. *Journal of Materials Chemistry* 1999;9:2251–8.
- [8] Milikian G, Rouessac FP, Alexander C. Synthesis of substituted dicyanomethylendihydrofurans. *Synthetic Communications* 1995;25:3045–51.
- [9] He M, Leslie TM, Sinicropi JA. Synthesis of chromophores with extremely high electro-optic activity. 1. Thiophene-bridge-based chromophores. *Chemistry of Materials* 2002;14:4662–8.
- [10] Bredereck H, Simchen G, Rebsdats S, Kantlehner W, Horn P, Wahl R, et al. Säureamidreaktionen, I; Orthoamide, I Darstellung und eigenschaften der amidacetale und aminalester. *Chemische Berichte* 1968;101:47–50.
- [11] Moon IK, Choi C-S, Kim N. Synthesis and characterization of novel photoconducting carbazole derivatives in main-chain polymers for photorefractive applications. *Polymer* 2007;48:3461–7.
- [12] Ahlmeim M, Barzoukas M, Bedworth PV, Blanchard-Desce M, Fort A, Hu ZY, et al. Chromophores with strong heterocyclic acceptors: a poled polymer with a large electro-optic coefficient. *Science* 1996;271:335.
- [13] He MQ, Leslie TM, Sinicropi JA, Garner SM, Reed LD. Synthesis of chromophores with extremely high electro-optic activities. 2. Isophorone- and combined isophorone-thiophene-based chromophores. *Chemistry of Materials* 2002;14:4669–75.
- [14] Dalton LR. Polymeric electro-optic materials: optimization of electro-optic activity, minimization of optical loss, and fine-tuning of device performance. *Optical Engineering* 2000;39:589–95.
- [15] Casado J, Pappenfus TM, Miler LL, Mann KR, Oriti E, Viruela PM, et al. Nitro-functionalized oligothiophenes as a novel type of electroactive molecular materials: spectroscopic, electrochemical, and computational study. *Journal of American Chemical Society* 2003;125:2524.
- [16] Effenberger F, Wuerthner F, Steybe F. Synthesis and solvatochromic properties of donor–acceptor-substituted oligothiophenes. *Journal of Organic Chemistry* 1995;60:2082.
- [17] Mata JA, Peris E, Asselberghs I, VanBoxel R, Persoons A. Large second-order NLO properties of new conjugated oligomers with a pendant ferrocenyl and an end-capped pyridine. *New Journal of Chemistry* 2001;25:1043.
- [18] Barlow S, Bunting HE, Ringham C, Green JC, Bubblitz GU, Boxer SG, et al. Studies of the electronic structure of metallocene-based second-order nonlinear optical dyes. *Journal of American Chemical Society* 1999;121:3715.
- [19] Grunnet-Jepsen A, Wright D, Smith B, Bratcher MS, DeClue MS, Siegel JS, et al. Spectroscopic determination of trap density in C_{60} -sensitized photorefractive polymers. *Chemical Physics Letters* 1998;291:553–61.
- [20] Bernède JC, Derouiche H, Djara V. Organic photovoltaic devices: influence of the cell configuration on its performances. *Solar Energy Materials & Solar Cells* 2005;87:261–70.
- [21] Frisch MJ, Trucks GW, Schlegel HB, Scuseria GE, Robb MA, Cheeseman JR, Zakrzewski VG, Montgomery Jr JA, Stratmann RE, Burant JC, Dapprich S, Millam JM, Daniels AD, Kudin KN, Strain MC, Farkas O, Tomasi J, Barone V, Cossi M, Cammi R, Mennucci B, Pomelli C, Adamo C, Clifford S, Ochterski J, Petersson GA, Ayala PY, Cui Q, Morokuma K, Malick DK, Rabuck AD, Raghavachari K, Foresman JB, Cioslowski J, Ortiz JV, Stefanov BB, Liu G, Liashenko A, Piskorz P, Komaromi I, Gomperts R, Martin RL, Fox DJ, Keith T, Al-Laham MA, Peng CY, Nanayakkara A, Gonzalez C, Challacombe M, Gill PMW, Johnson B, Chen W, Wong MW, Andres JL, Head-Gordon M, Replogle ES, Pople JA. GAUSSIAN 98. Pittsburgh, PA: Gaussian, Inc.; 1998.
- [22] Wu X, Wu J, Liu YQ, Jen AKY. Highly efficient, thermally and chemically stable second order nonlinear optical chromophores containing a 2-phenyl-tetra-cyanobutadienyl acceptor. *Journal of American Chemical Society* 1999;121:472.
- [23] Zhang C, Ren AS, Wang F, Zhu J, Dalton LR. Synthesis and characterization of sterically stabilized second-order nonlinear optical chromophores. *Chemistry of Materials* 1999;11:1966.
- [24] Van Walree CA, Franssen O, Marsman AW, Flipse MC, Jenneskens LW. Second-order nonlinear optical properties of stilbene, benzylideneaniline and azobenzene derivatives. The effect of π -bridge nitrogen insertion on the first hyperpolarizability. *Journal of the Chemical Society, Perkin Transactions* 1997;2:799–808.
- [25] Wortmann R, Glania C, Kraemer P, Lukaszuk K, Matshiner R, Twieg RJ, et al. Highly transparent and birefringent chromophores for organic photorefractive materials. *Chemical Physics* 1999;245:107–20.
- [26] Marder SR, Perry JW, Bourhill G, Gorman CV, Tiemann BG, Mansour K. Relation between bond-length alternation and second electronic hyperpolarizability of conjugated organic molecules. *Science* 1993;261:186–9.
- [27] Chen G, Lu D, Gooddard WA. Valence-bond charge-transfer solvation model for nonlinear optical properties of organic molecules in polar solvents. *Journal of Chemical Physics* 1994;101:5860–4.
- [28] Chemla DS, Zyss J. Non-linear optical properties of organic molecular and crystals, vols. 1 and 2. Orlando: Academic Press; 1987.
- [29] Kamlet MJ, Abboud JLM, Abraham MH, Taft RW. Linear solvation energy relationships. 23. A comprehensive collection of the solvatochromic parameters, π^* , α , and β , and some methods for simplifying the generalized solvatochromic equation. *Journal of Organic Chemistry* 1983;48:2877. and references cited therein.

Abbreviations

ATOP: 1-alkyl-5-[2-(5-dialkylaminothienyl)methylene]-4-alkyl-[2,6-dioxo-1,2,5,6-tetrahydropyridine]-3-carbonitrile
 CV: cyclic voltammetry
 DMF: N,N'-dimethylformamide
 DMNPAA: 2,5-dimethyl-4-(p-nitrophenylazo)anisole
 EO: electro-optic, electro-optical
 FOM: figure-of-merit
 HF: Hatree–Fock
 HOMO: highest occupied molecular orbital
 LUMO: lowest unoccupied molecular orbital
 MOPAC: Molecular Orbital Package
 NLO: nonlinear optical
 PM3: Parameterization Model 3
 PR: photorefractive
 PVK: poly(N-vinylcarbazole)
 THF: tetrahydrofuran
 T_g: glass transition temperature